Tunable Three-Body Loss in a Nonlinear Rydberg Medium

D. P. Ornelas-Huerta,[1,*] Przemyslaw Bienias,[1,2,*] Alexander N. Craddock,[1] Michael J. Gullans,[1,2,3] Andrew J. Hachtel,[1] Marcin Kalinowski,[1,4] Mary E. Lyon,[1] Alexey V. Gorshkov,[1,2] S. L. Rolston,[1] and J. V. Porto[1]

[1]*Joint Quantum Institute, NIST/University of Maryland, College Park, Maryland 20742, USA*

[2]*Joint Center for Quantum Information and Computer Science, NIST/University of Maryland, College Park, Maryland 20742, USA*

[3]*Department of Physics, Princeton University, Princeton, New Jersey 08544, USA*

[4]*Faculty of Physics, University of Warsaw, Pasteura 5, 02-093 Warsaw, Poland*

(Received 29 September 2020; accepted 2 February 2021; published 26 April 2021)

Long-range Rydberg interactions, in combination with electromagnetically induced transparency (EIT), give rise to strongly interacting photons where the strength, sign, and form of the interactions are widely tunable and controllable. Such control can be applied to both coherent and dissipative interactions, which provides the potential for generating novel few-photon states. Recently it has been shown that Rydberg-EIT is a rare system in which three-body interactions can be as strong or stronger than two-body interactions. In this work, we study three-body scattering loss for Rydberg-EIT in a wide regime of single and two-photon detunings. Our numerical simulations of the full three-body wave function and analytical estimates based on Fermi's golden rule strongly suggest that the observed features in the outgoing photonic correlations are caused by the resonant enhancement of the three-body losses.

DOI: 10.1103/PhysRevLett.126.173401

Photons coherently coupled to highly excited atoms in the form of dark-state Rydberg polaritons are a versatile system for engineering strong interactions between photons. Recent experiments have shown single-photon nonlinearities [1–7], single-photon transistors [8–10], quantum gates [11–14], as well as the observation of strongly correlated photon states [15–17]. Depending on the conditions used to generate the polaritons, the interactions can be coherent or dissipative, with controllable inherent multibody character [18–24]. The study of few-body systems with long-range interactions can help to engineer more complex many-body quantum systems and understand their properties and potential limitations due to loss, decoherence, or recombination. Realizing precise and reliable control of three-body effects opens the door to rich phenomena, such as the universality of Efimov states [25], the purification of a quantum gas [26], and the emergence of strongly correlated photonic states [16,17], including fractional quantum Hall states [27,28]. Dissipative interactions find applications in quantum computing and state preparation [29,30], and in passive quantum error correction [31–33]. In particular, three-body dissipative interactions enable preparation of strongly correlated [34] and topological phases [35].

Three-body effects between Rydberg polaritons can be strong [16,17,21–23], distinguishing them from the usually weak three-body forces [36] observed with ultracold atoms and molecules near their ground state [34,37–39]. The three-body Rydberg polariton system has been explored experimentally in the dispersive regime [16,17]. However, to our knowledge, there is no theoretical or experimental work studying dissipative three-body interactions and their tunability to date.

Here, we analyze tunable three-body loss of Rydberg polaritons at high optical density, where nonperturbative effects are strong. We study experimentally and theoretically, the tunability of the relative strength of three-body loss versus two-body loss, which is indirectly probed by measuring two- and three-photon correlation functions.

Figure 1(a) shows the atomic-level configuration for Rydberg EIT. The ground state $|G\rangle$ of an ensemble of atoms is coupled to an intermediate state $|P\rangle$ by a quantum probe light with a collective coupling strength g. A classical control field with Rabi frequency Ω_c couples $|P\rangle$ to a Rydberg state $|S\rangle$. The Hamiltonian describing the propagation of a single excitation is [19,40]

$$H = \begin{pmatrix} cq & g & 0 \\ g & -\Delta - \delta_s & \Omega_c/2 \\ 0 & \Omega_c/2 & -\Delta_s \end{pmatrix}, \tag{1}$$

in the basis of $\{\mathcal{E}, P, S\}$, where $\mathcal{E}$, P, and S are the wave functions of the photonic component, intermediate-, and Rydberg-state collective spin excitations, respectively [40] ($\hbar = 1$). The complex detunings $\Delta = \delta + i\Gamma/2$ and $\Delta_s = \delta_s + i\gamma_s/2$ take into account the decay rates of the excited states, cq corresponds to the kinetic energy of the photon in the rotating frame (such that the incoming probe photons have zero energy), where c is the speed of light, and q is the probe photon momentum. Diagonalization of Eq. (1) gives rise to three polariton eigenstates. For small δ_s, the photons

 © 2021 American Physical Society

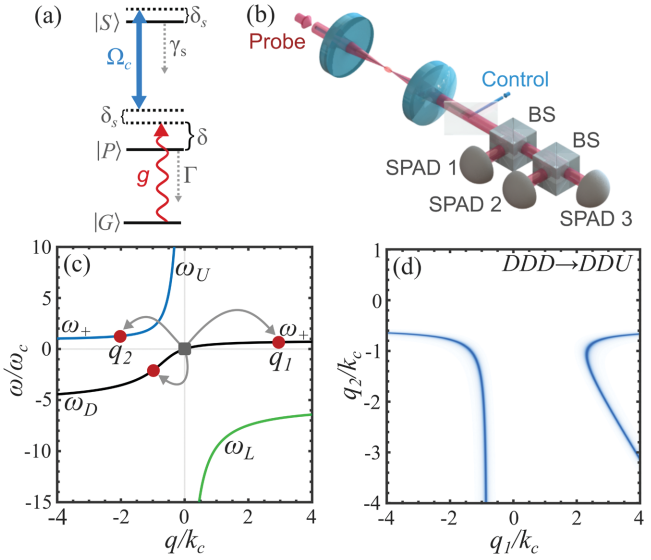

FIG. 1. (a) Atomic structure: A weak probe, with collectively enhanced single-photon coupling g, and a classical field, with Rabi frequency Ω_c, couple the ground state, $|G\rangle = |5S_{1/2}, F = 2, m_F = 2\rangle$, to the Rydberg state $|S\rangle = |82S_{1/2}, m_J = 1/2\rangle$ via an intermediate state $|P\rangle = |5P_{3/2}, F = 3, m_F = 3\rangle$. (b) Experimental setup: The probe and control beams are overlapped along the propagation axis. After exiting the atomic medium, the probe beam is sent to a generalized Hanbury Brown–Twiss setup to measure the photon correlation functions. (c) Dispersion of polaritons in the limit $\Gamma \ll |\delta|$, with $\delta/(2\pi) = 25$ MHz, $\delta_s/(2\pi) = 0$, $\Omega_c/(2\pi) = 23.5$ MHz, for a homogeneous cloud of length $L = 4.2\sigma_z$ [15], with $\omega_c \equiv \Omega_c^2/4|\Delta|$ and $k_c \equiv \omega_c/v_g \approx g^2/c|\Delta|$. The black curve is the dark-state branch (D), while the blue and green curves are the bright states (U and L). The diagram depicts the allowed three-body loss process for three polaritons initially near the EIT resonance at $\omega_j = q_j = 0$ ($j = 1, 2, 3$ labels the three polaritons). ω_+ is the energy where ω_D and ω_U become approximately flat. (d) Allowed final momenta q_1 and q_2 for the three-body loss with $q_3 = -q_1 - q_2$. Only the process depicted in (c) is relevant for $\delta_s \approx 0$. For the plotted momenta, there is no two-body loss process allowed because there are no final states with $q_1 = 0$ or $q_2 = 0$.

propagate through the medium as dark-state polaritons: a hybrid photon-atom excitation with a negligible admixture of the lossy intermediate state [41]. This coupling maps the strong Rydberg interaction onto the photons [18,42].

Figure 1(c) depicts the energies of the dark D, bright lower L, and bright upper U, polaritons [depicted by $\omega_D(q)$, $\omega_L(q)$, and $\omega_U(q)$, respectively]. The middle branch D is continuously connected to the dark state; however, for large momenta $|q|$, it becomes lossy.

For small $|\delta_s| \ll \omega_c \equiv \Omega_c^2/4|\Delta|$, two-body scattering processes where one or both of the incoming dark polaritons become lossy are strongly suppressed [19], see Fig. 1(d) illustrating the $DD \to DU$ suppression. This suppression comes from the fact that, for $\delta_s = 0$, incoming $q = 0$ polaritons are not allowed to scatter to any bright channel due to energy and momentum conservation.

However, for three photons, the scattering to lossy branches is allowed by conservation laws. The interplay of the shape of the interactions and the dispersion relation can lead to resonant enhancement of three-body loss. Both the interaction potential and the dispersion relation can be tuned using Ω_c, δ, and δ_s, which we explore experimentally and theoretically.

We generate Rydberg polaritons in a cold, optically trapped cloud of ^{87}Rb atoms using the three states $|G\rangle = |5S_{1/2}, F = 2, m_F = 2\rangle$, $|P\rangle = |5P_{3/2}, F = 3, m_F = 3\rangle$, and $|S\rangle = |82S_{1/2}, m_J = 1/2\rangle$ (see Supplemental Material [43]). The probe beam addressing the $|G\rangle$-$|P\rangle$ transition has a 3.3 μm-waist and coupling strength $g/(2\pi) \simeq 10^3$ MHz. The average incoming photon rate is $R_{\rm in} \simeq 3\ \mu s^{-1}$, so the likelihood of more than three photons in the cloud is negligible. The control beam coupling $|P\rangle$-$|S\rangle$ is counterpropagating to the probe [Fig. 1(b)] with a 19 μm-waist and $\Omega_c/(2\pi) = 23.5 \pm 1.5$ MHz. The ensemble with $\simeq 10^5$ atoms at 10 μK has an rms axial length of $\sigma_z = 42 \pm 4$ μm. The optical depth is OD $= 37 \pm 4$, and we measure the linewidths to be $\Gamma/(2\pi) = 7 \pm 1$ and $\gamma_s/(2\pi) = 0.4 \pm 0.1$ MHz [47].

The impact of interactions among n polaritons can be characterized by the n-photon correlation functions, $g^{(2)}(\tau)$ and $g^{(3)}(\tau_1, \tau_2)$ for $n = 2$ and $n = 3$, respectively. We measure these correlations by detecting the relative temporal delay τ of transmitted photons using three single-photon avalanche photodetectors (SPAD) [see Fig. 1(b)]. To characterize the impact of three-body loss relative to two-body effects at low photon rates, we use the connected correlation [17,21]

$$\eta_3(\tau_1, \tau_2) = g^{(2)}(\tau_1) + g^{(2)}(\tau_2) + g^{(2)}(\tau_2 - \tau_1) - g^{(3)}(\tau_1, \tau_2) - 2. \quad (2)$$

For dominant two-body loss, one has $\eta_3(0,0) < 0$, because there is a high probability of absorbing at least one out of two or three incoming photons so $g^{(2)}(0)$ and $g^{(3)}(0,0)$ are suppressed (strong two-body repulsion [7] has a similar effect).

On the other hand, if two-body loss is small and dispersive, so two-body interactions are weak or attractive such that $g^{(2)}(0) \geq 1$, while three-body loss is strong, $\eta_3(0,0) > 0$. Therefore, we use a positive value of $\eta_3(0,0)$ as a signature of strong three-body losses. Figure 2 shows the measured second-order, third-order, and connected third-order correlation functions for two parameter choices corresponding to $\eta_3(0,0) < 0$ [Figs. 2(a)–2(c)] and $\eta_3(0,0) > 0$ [Figs. 2(d)–2(f)].

Figures 3(a)–3(c) show the measured correlation functions, $g^{(2)}(0)$, $g^{(3)}(0,0)$, and $\eta_3(0,0)$, as a function of δ and δ_s, at fixed Ω_c. The region where $\eta_3(0,0) > 0$ (indicative of dominant three-body loss) occurs is a roughly linear band in $\delta - \delta_s$ space with a negative slope. Figures 3(d)–3(f) show $g^{(2)}(0)$, $g^{(3)}(0,0)$, and $\eta_3(0,0)$ obtained by

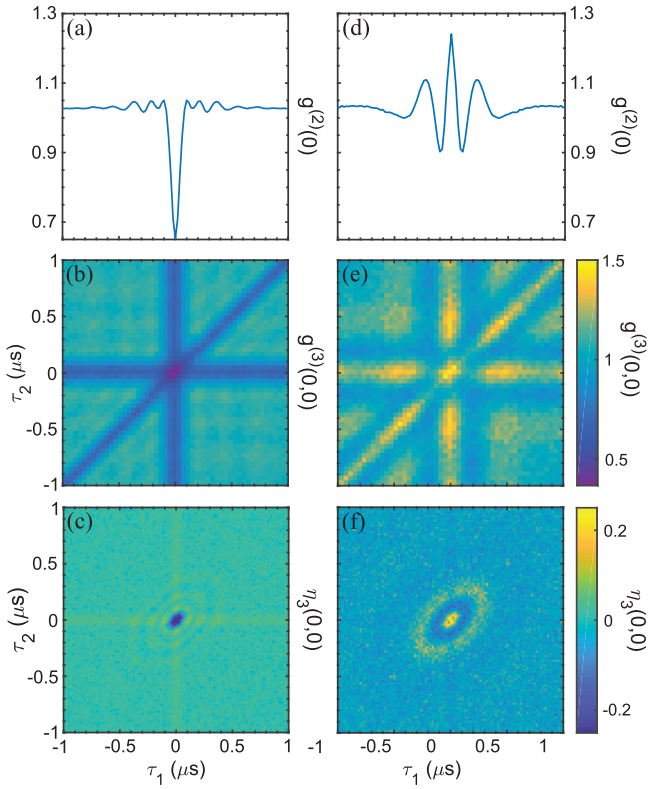

FIG. 2. (a)–(c) Measured (a) $g^{(2)}(\tau)$, (b) $g^{(3)}(\tau_1,\tau_2)$, and (c) $\eta_3(\tau_1,\tau_2)$ for the experimental parameters indicated in the text with $\delta/(2\pi) = 15$ and $\delta_s/(2\pi) = -2$ MHz, where $\eta_3(0,0) < 0$. (d)–(f) Measured (d) $g^{(2)}(\tau)$, (e), $g^{(3)}(\tau_1,\tau_2)$, and (f) $\eta_3(\tau_1,\tau_2)$ for $\delta/(2\pi) = 22.5$ and $\delta_s/(2\pi) = 2$ MHz, where $\eta_3(0,0) > 0$.

numerically solving the Schrödinger equation for the two- and three-polariton wave functions propagating through the Rydberg-EIT medium using parameters similar to the experimental values [48]. We find good qualitative agreement between the numerical calculation and experiment: we reproduce the antibunching to bunching behavior in $g^{(2)}(0)$ and $g^{(3)}(0,0)$, and the resonantlike feature of three-body loss in $\eta_3(0,0)$. We note that limitations from our numerical description arise from using a hard-sphere approximation for the interaction potential, possibly contributing to the discrepancy between experimental and numerical results. Other possible sources of discrepancy include experimental drifts and the presence of contaminant states [49]. The latter causes a bunching feature for long times in the correlation functions [50]. Including a microscopic description of the contaminants would greatly increase the complexity of the numerical and theoretical model [51].

Rydberg atoms interact via the van der Waals potential $V(r) = C_6/r^6$. The effective interaction between two dark-state polaritons (after integrating out bright-state polaritons) is [19]

$$V_e(\omega, r) = \frac{V(r)}{1 - \bar{\chi}(\omega)V(r)}. \tag{3}$$

Here, ω is the total energy of the incoming polaritons and $\bar{\chi}$ characterizes the saturation of the potential at distances less than the blockade radius $r_b = (C_6|\bar{\chi}|)^{1/6}$ [19] and is given by

$$\bar{\chi}(\omega) = \frac{-\Omega_c^2 + 4\tilde{\Delta}^2 + 6\tilde{\Delta}\nu + 2\nu^2}{2(\tilde{\Delta} + \nu)(\nu(2\tilde{\Delta} + \nu) - \Omega_c^2)} \tag{4}$$

with $\nu = \omega + 2\Delta_s$ and $\tilde{\Delta} = \delta + i\Gamma/2 - i\gamma_s/2$. Since $\gamma_s \ll \Gamma$, we neglect the difference between $\tilde{\Delta}$ and $\Delta = \delta + i\Gamma/2$. In our experiment, r_b ranges from 7 to 10 μm. Note that with decreasing δ, the effect on $g^{(2)}(0)$ of the two-body dissipation in V_e (coming from Γ via $\bar{\chi}$) becomes stronger, leading—in combination with competing attractive dispersive interactions—to the decrease of $g^{(2)}(0)$, see Figs, 3(a),3(d).

Using V_e, we analyze the three-body scattering rate β, for incoming dark-state polaritons near EIT resonance due to processes like the one indicated in Fig. 1(c). We perform

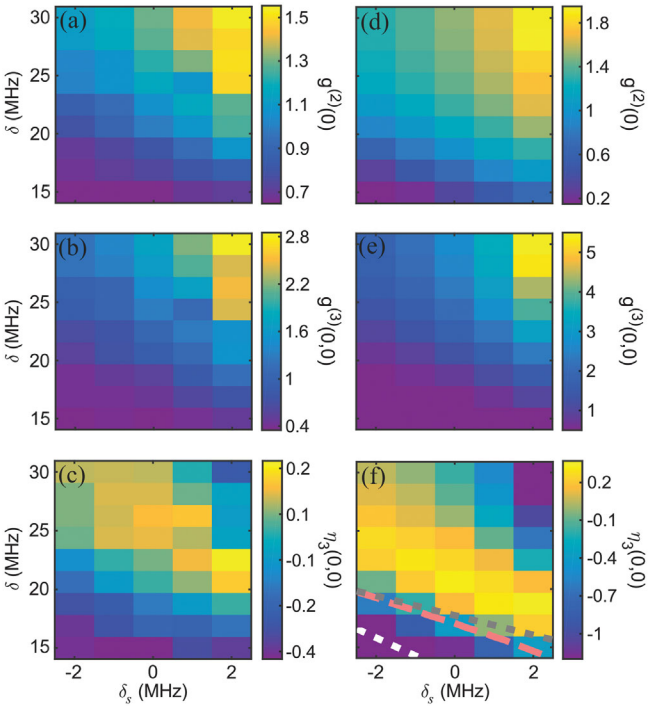

FIG. 3. (a)–(c) Experimental data of the second-order $g^{(2)}(0)$, third-order $g^{(3)}(0,0)$, and connected $\eta_3(0,0)$ correlation functions with $\Omega_c/(2\pi) = 23.5 \pm 1.5$ MHz, for a cloud with OD $= 37 \pm 4$ and $\sigma_z = 42 \pm 4$ μm. (d)–(f) Numerical simulations for the same correlation functions. Parameters used for the simulations are OD $= 37$, $\Omega_c/2\pi = 25$ MHz, $\Gamma/2\pi = 7$ MHz, $\gamma/2\pi = 0.3$ MHz, and $\sigma_z = 40$ μm. Regions with $\eta_3(0,0) > 0$ indicate excess of three-body loss with respect to two-body loss. The dashed lines indicate enhanced three-body loss predicted by Fermi's golden rule calculation (see text).

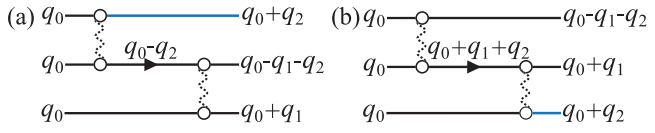

FIG. 4. Lowest-order diagrams that contribute to three-body loss. The black lines indicate polaritons in the dark branch, and the blue lines indicate polaritons scattered to the upper-bright branch. Dotted-wiggly lines indicate the effective pairwise interactions. We use the full propagator for the S states in the virtual state (black-arrowed line), which includes contributions from all branches. Additionally, five similar diagrams (total of six) for both (a)–(b) are obtained by permuting inputs and outputs.

our analysis in the limit of zero dissipation and then analytically continue to finite Γ and γ_s.

The lowest-order diagrams contributing to β are second order in V_e. The conservation of energy and momentum puts additional restrictions on the available open scattering channels. In Figs. 4(a)–4(b), we show the leading contributions to β which involve scattering to DDU with D gaining large q and becoming lossy. We neglect other allowed processes, such as scattering to DUL due to the weaker effective interactions involving these bright polaritons because of their small Rydberg amplitude.

The incoming polaritons have $\omega_D(q_0) = 0$. In general, the incoming momentum $q_0 \neq 0$ for $\delta_s \neq 0$, but, for brevity, we show the expressions for $\delta_s = 0$ and $q_0 = 0$. Within a Fermi's golden rule calculation, the diagrams in Figs. 4(a) and 4(b) contribute, respectively, the first and second terms inside the absolute value in the expression for β:

$$\begin{aligned}\beta = \frac{18}{\pi}\int \mathrm{d}q_1\mathrm{d}q_2 |S_D^0|^6 |S_D^{q_1}|^2 |S_D^{-q_1-q_2}|^2 |S_U^{q_2}|^2 \\ \times |\tilde{V}_{q_2}[0]G_{ss}[-q_2, -\omega_U(q_2)]\tilde{V}_{q_1}[-\omega_U(q_2)] \\ + \tilde{V}_{q_1+q_2}[0]G_{ss}[q_1+q_2, -\omega_D(-q_1-q_2)] \\ \times \tilde{V}_{q_2}[-\omega_D(-q_1-q_2)]|^2 \\ \times \delta[\omega_U(q_2) + \omega_D(q_1) + \omega_D(-q_1-q_2)]. \end{aligned} \tag{5}$$

Here, $\tilde{V}_q[\omega]$ is the Fourier transform of $V_e(\omega, r)$, G_{ss} is the single-body propagator projected onto the Rydberg state, $\omega_U(q)$ is the dispersion for the upper-bright branch, and S_ν^q is the overlap of the Rydberg state with a polariton at momentum q on branch $\nu \in \{D, U\}$ (see Supplemental Material [43]).

The behavior of Eq. (5) depends on the interaction strength, which can be quantified by $\varphi = |r_b/\sqrt{\bar{\chi}/m}|$, where $m = -2g^4/\Delta\Omega^2c^2$. For $|\delta| \gg \Omega_c/2$, φ simplifies to $\mathrm{OD}_b\Gamma/4|\Delta|$ (which, up to a constant factor, is the phase a stationary Rydberg excitation imprints on a passing polariton [18]), where $\mathrm{OD}_b = \mathrm{OD}r_b/\sqrt{2\pi}\sigma_z$ is the optical depth per blockade radius corresponding to the maximal density of a Gaussian cloud with rms σ_z. In our experiment, OD_b is < 4, thus for the detunings considered here $\varphi < 0.3$.

In our experimental regime, with moderately strong interactions ($\varphi < 1$), we can simplify Eq. (5) by noting that the dispersions for ω_D and ω_U saturate to ω_+ (see Ref. [43]) in the relevant range of the momentum transfer $\sim 1/r_b$ being larger than the characteristic threshold momentum $k_c \equiv \omega_c/v_g$, where v_g is the group velocity [see Figs. 1(c),1(d)].

Then, the second term in Eq. (5) vanishes because $\tilde{V}_{q_2}[-\omega_D(-q_1-q_2)] \approx \tilde{V}_{q_2}[2\omega_+] \to 0$, so β simplifies to [52]

$$\frac{18}{\pi}\int \mathrm{d}q \frac{1}{v_g(-2\omega_+)} |\tilde{V}_q[0]G_{ss}[q_2 \to \infty, -\omega_+]\tilde{V}_q[-\omega_+]|^2, \tag{6}$$

which has a complicated dependence on the experimental parameters. We concentrate on qualitative features of Eq. (6) to understand the behavior of β. For $\Omega_c \ll |\delta|$, the scattering rate is reduced to $\beta \propto \varphi r_b^2\Omega_c^2/\delta$. Here, β increases with φ, but does not feature any resonances as a function of δ.

In contrast, for $\Omega_c \sim \delta$, Eq. (6) could have resonant behavior for two reasons. First, the density of outgoing states, characterized by $1/v_g(-2\omega_+)$, could diverge as a function of δ. Second, the interaction vertices $\tilde{V}_q[0]$ or $\tilde{V}_q[-\omega_+]$, which are inversely proportional to $\bar{\chi}(0)$ and $\bar{\chi}(-\omega_+)$, could have a resonance due to the vanishing value of $\bar{\chi}$. This divergence in the interaction vertices will be smoothed out for finite Γ, γ_s, but will still have a significant impact on β. We find that the divergence in the density of states is nearly canceled by the simultaneous vanishing of $\tilde{V}_q[-\omega_+]$ (see Supplemental Material [43]), so the density of states does not contribute to the resonance.

The interaction vertices $\tilde{V}_q[0]$ and $\tilde{V}_q[-\omega_+]$ diverge for δ approaching specific respective detunings δ_0 and δ_+ where $\bar{\chi}(0)$ and $\bar{\chi}(-\omega_+)$ vanish, respectively. In the experimentally relevant limit $|\delta_s| \ll \Omega_c, |\Delta|$, the expressions for δ_0 and δ_+ simplify to $\delta_0 = \frac{1}{2}\Omega_c - (3/2)\delta_s$, $\delta_+ \approx 0.7\Omega_c - 0.8\delta_s$. Figure 3(f) shows these dependencies: the gray-dotted line depicts δ_+, whereas the white-dotted line depicts δ_0. The decay Γ leads to such significant broadening of the two resonances that the two peaks are no longer distinguishable, leading to a single, effective resonant feature for β. In Fig. 3(f), the pink-dashed curve depicts the value of δ for which $|\beta|$ is maximal for a fixed δ_s.

The maximal curve is closer to the δ_+ line because, for our parameters, this resonance is stronger than the δ_0 resonance. The resulting overall resonance is a three-body effect because it predominantly comes from the δ_+ resonance, which is not present for the two-body scattering. In the vicinity of a divergent $1/\bar{\chi}$, the interaction strength

could become large and negative, leading to a second bound state, which would happen for $\varphi \approx 3$ [19]. This nonperturbative effect could hinder the applicability of Fermi's golden rule. However, since in our system $\varphi < 0.3$ (due to dissipation), we neglect the second bound state.

The measured three-body scattering probes nonperturbative processes, even in the moderately interacting regime for $\varphi < 1$. In this moderately interacting regime Fermi's golden rule calculation is approximate—it involves a resummation strategy to perform perturbation theory in the effective two-body interaction. This approximation likely contributes to the discrepancy between our perturbative analysis and numerical simulations. Similar to the problem of describing Efimov bound states [25], nonperturbative effects can be more accurately captured by introducing an effective three-body interaction between dark-state polaritons [16,21,22]. These N-body interactions, however, are a momentum and frequency-dependent quantity in free space, whose full description requires the exact solution to the N-body problem. Steps toward developing an approximate, consistent renormalization group treatment of three-body forces have recently been made by analyzing single-mode-cavity setups [53].

Summary and outlook.—We demonstrate the ability to tune Rydberg-polariton interactions leading to resonantly enhanced three-body losses. These interactions are analyzed using the few-body auto-correlation functions of the outgoing field. Our numerical simulations reproduce the observed features with good qualitative agreement. We describe the tunable losses based on Fermi's golden rule treatment of the scattering process of three dark-state polaritons to two lossy dark-state polaritons and a bright-state polariton. One way of increasing the overall strength of all involved interactions and three-body loss is by increasing the optical depth per blockade radius. Also, decreasing the dissipation from the decay of the intermediate and Rydberg states would make the resonant feature stronger and narrower since these decays lead to the imaginary parts of the potentials broadening the resonances. This can be achieved by simultaneously increasing the Rabi frequency and the single-photon detuning such that the resonance is still present, but suppressing the dissipative part of the interactions as $\Gamma/|\delta|$. However, the optical power needed to achieve strong enough Rabi frequencies can be experimentally challenging. Furthermore, nonperturbative effects will be enhanced (like the appearance of a second bound state), making the theoretical analysis more complex. Pushing further into this regime would enable the production of a novel three-photon number filter.

Our work demonstrates the tunability of Rydberg systems, showing promising directions in the study and control of few and many-body physics of strongly interacting photons, with potential applications in quantum information, quantum simulation, and exploration of exotic phases of matter with controllable interactions. For example, another bound state could emerge with a higher OD_b [19]; these additional bound states could be used as another tuning knob to increase three-body forces. Extending the system to three dimensions and altering the polariton effective longitudinal and transverse mass and interactions, could result in photonic Efimov trimers [23]. Another exciting direction involves studying unconventional topological and spin-liquid phases with three-body forces, especially in two dimensions [54].

We thank Hans Peter Büchler, Yidan Wang, and Elizabeth Goldschmidt for insightful discussion. We are also grateful to Nathan Fredman for his contributions to the experiment. P. B., M. K., A. C, D. O.-H, S. L. R., J. V. P., and A. V. G. acknowledge support from the United States Army Research Lab's Center for Distributed Quantum Information (CDQI) at the University of Maryland and the Army Research Lab, and support from the National Science Foundation Physics Frontier Center at the Joint Quantum Institute (Grant No. PHY1430094). P. B., M. K., and A. V. G. additionally acknowledge support from AFOSR, ARO MURI, AFOSR MURI, DOE ASCR Quantum Testbed Pathfinder program (Award No. DE-SC0019040), U.S. Department of Energy Award No. DE-SC0019449, DOE ASCR Accelerated Research in Quantum Computing program (Award No. DE-SC0020312), and NSF PFCQC program. M. K. acknowledges financial support from the Foundation for Polish Science within the First Team program co-financed by the European Union under the European Regional Development Fund.

[*] These authors contributed equally to this work.

[1] A. K. Mohapatra, T. R. Jackson, and C. S. Adams, Phys. Rev. Lett. **98**, 113003 (2007).
[2] Y. O. Dudin and A. Kuzmich, Science **336**, 887 (2012).
[3] T. Peyronel, O. Firstenberg, Q.-Y. Liang, S. Hofferberth, A. V. Gorshkov, T. Pohl, M. D. Lukin, and V. Vuletić, Nature (London) **488**, 57 (2012).
[4] D. Maxwell, D. J. Szwer, D. Paredes-Barato, H. Busche, J. D. Pritchard, A. Gauguet, K. J. Weatherill, M. P. A. Jones, and C. S. Adams, Phys. Rev. Lett. **110**, 103001 (2013).
[5] L. Li and A. Kuzmich, Nat. Commun. **7**, 13618 (2016).
[6] A. Paris-Mandoki, C. Braun, J. Kumlin, C. Tresp, I. Mirgorodskiy, F. Christaller, H. P. Büchler, and S. Hofferberth, Phys. Rev. X **7**, 041010 (2017).
[7] S. H. Cantu, A. V. Venkatramani, W. Xu, L. Zhou, B. Jelenković, M. D. Lukin, and V. Vuletić, Nat. Phys. **16**, 921 (2020).
[8] H. Gorniaczyk, C. Tresp, J. Schmidt, H. Fedder, and S. Hofferberth, Phys. Rev. Lett. **113**, 053601 (2014).
[9] D. Tiarks, S. Baur, K. Schneider, S. Dürr, and G. Rempe, Phys. Rev. Lett. **113**, 053602 (2014).
[10] H. Gorniaczyk, C. Tresp, P. Bienias, A. Paris-Mandoki, W. Li, I. Mirgorodskiy, H. P. Büchler, I. Lesanovsky, and S. Hofferberth, Nat. Commun. **7**, 12480 (2016).

[11] K. M. Maller, M. T. Lichtman, T. Xia, Y. Sun, M. J. Piotrowicz, A. W. Carr, L. Isenhower, and M. Saffman, Phys. Rev. A **92**, 022336 (2015).

[12] Y. Zeng, P. Xu, X. He, Y. Liu, M. Liu, J. Wang, D. J. Papoular, G. V. Shlyapnikov, and M. Zhan, Phys. Rev. Lett. **119**, 160502 (2017).

[13] H. Levine, A. Keesling, A. Omran, H. Bernien, S. Schwartz, A. S. Zibrov, M. Endres, M. Greiner, V. Vuletić, and M. D. Lukin, Phys. Rev. Lett. **121**, 123603 (2018).

[14] D. Tiarks, S. Schmidt-Eberle, T. Stolz, G. Rempe, and S. Dürr, Nat. Phys. **15**, 124 (2019).

[15] O. Firstenberg, T. Peyronel, Q.-Y. Liang, A. V. Gorshkov, M. D. Lukin, and V. Vuletić, Nature (London) **502**, 71 (2013).

[16] Q.-Y. Liang, A. V. Venkatramani, S. H. Cantu, T. L. Nicholson, M. J. Gullans, A. V. Gorshkov, J. D. Thompson, C. Chin, M. D. Lukin, and V. Vuletić, Science **359**, 783 (2018).

[17] N. Stiesdal, J. Kumlin, K. Kleinbeck, P. Lunt, C. Braun, A. Paris-Mandoki, C. Tresp, H. P. Büchler, and S. Hofferberth, Phys. Rev. Lett. **121**, 103601 (2018).

[18] A. V. Gorshkov, J. Otterbach, M. Fleischhauer, T. Pohl, and M. D. Lukin, Phys. Rev. Lett. **107**, 133602 (2011).

[19] P. Bienias, S. Choi, O. Firstenberg, M. F. Maghrebi, M. Gullans, M. D. Lukin, A. V. Gorshkov, and H. P. Büchler, Phys. Rev. A **90**, 053804 (2014).

[20] M. Moos, M. Höning, R. Unanyan, and M. Fleischhauer, Phys. Rev. A **92**, 053846 (2015).

[21] K. Jachymski, P. Bienias, and H. P. Büchler, Phys. Rev. Lett. **117**, 053601 (2016).

[22] M. J. Gullans, J. D. Thompson, Y. Wang, Q.-Y. Liang, V. Vuletić, M. D. Lukin, and A. V. Gorshkov, Phys. Rev. Lett. **117**, 113601 (2016).

[23] M. J. Gullans, S. Diehl, S. T. Rittenhouse, B. P. Ruzic, J. P. D'Incao, P. Julienne, A. V. Gorshkov, and J. M. Taylor, Phys. Rev. Lett. **119**, 233601 (2017).

[24] F. M. Gambetta, C. Zhang, M. Hennrich, I. Lesanovsky, and W. Li, Phys. Rev. Lett. **125**, 133602 (2020).

[25] V. Efimov, Phys. Lett. **33B**, 563 (1970).

[26] L. H. Dogra, J. A. P. Glidden, T. A. Hilker, C. Eigen, E. A. Cornell, R. P. Smith, and Z. Hadzibabic, Phys. Rev. Lett. **123**, 020405 (2019).

[27] A. Wójs, C. Tőke, and J. K. Jain, Phys. Rev. Lett. **105**, 196801 (2010).

[28] B. Yang, Phys. Rev. B **98**, 201101(R) (2018).

[29] S. Diehl, A. Micheli, A. Kantian, B. Kraus, H. P. Büchler, and P. Zoller, Nat. Phys. **4**, 878 (2008).

[30] F. Verstraete, M. M. Wolf, and J. Ignacio Cirac, Nat. Phys. **5**, 633 (2009).

[31] D. A. Lidar, I. L. Chuang, and K. B. Whaley, Phys. Rev. Lett. **81**, 2594 (1998).

[32] B. M. Terhal, Rev. Mod. Phys. **87**, 307 (2015).

[33] S. Lieu, R. Belyansky, J. T. Young, R. Lundgren, V. V. Albert, and A. V. Gorshkov, Phys. Rev. Lett. **125**, 240405 (2020).

[34] A. J. Daley, J. M. Taylor, S. Diehl, M. Baranov, and P. Zoller, Phys. Rev. Lett. **102**, 040402 (2009).

[35] M. Roncaglia, M. Rizzi, and J. I. Cirac, Phys. Rev. Lett. **104**, 096803 (2010).

[36] For a recent proposal showing how to enhance three-body interactions between atoms in optical potentials, see Ref. [55].

[37] H. P. Büchler, E. Demler, M. Lukin, A. Micheli, N. Prokof'ev, G. Pupillo, and P. Zoller, Phys. Rev. Lett. **98**, 060404 (2007).

[38] P. R. Johnson, E. Tiesinga, J. V. Porto, and C. J. Williams, New J. Phys. **11**, 093022 (2009).

[39] L. Mazza, M. Rizzi, M. Lewenstein, and J. I. Cirac, Phys. Rev. A **82**, 043629 (2010).

[40] M. Fleischhauer and M. D. Lukin, Phys. Rev. Lett. **84**, 5094 (2000).

[41] M. Fleischhauer and M. D. Lukin, Phys. Rev. A **65**, 022314 (2002).

[42] D. Petrosyan, J. Otterbach, and M. Fleischhauer, Phys. Rev. Lett. **107**, 213601 (2011).

[43] See Supplemental Material at http://link.aps.org/supplemental/10.1103/PhysRevLett.126.173401 for experimental methods and theoretical details on Fermi's Golden Rule calculation and the associated analytical expressions, which includes Refs. [44–46].

[44] S. Rosi, A. Burchianti, S. Conclave, D. S. Naik, G. Roati, C. Fort, and F. Minardi, Sci. Rep. **8**, 1301 (2018).

[45] S. de Léséleuc, D. Barredo, V. Lienhard, A. Browaeys, and T. Lahaye, Phys. Rev. A **97**, 053803 (2018).

[46] The identification of commercial products in this Letter does not imply recommendation or endorsement by the National Institute of Standards and Technology nor does it imply that the items identified are necessarily the best available for the purpose.

[47] All uncertainties are statistical deviations.

[48] See Ref. [56] for details on the numerical simulation of the photonic correlation functions.

[49] P. Bienias, J. Douglas, A. Paris-Mandoki, P. Titum, I. Mirgorodskiy, C. Tresp, E. Zeuthen, M. J. Gullans, M. Manzoni, S. Hofferberth, D. Chang, and A. V. Gorshkov, Phys. Rev. Research **2**, 033049 (2020).

[50] D. P. Ornelas-Huerta, A. N. Craddock, E. A. Goldschmidt, A. J. Hachtel, Y. Wang, P. Bienias, A. V. Gorshkov, S. L. Rolston, and J. V. Porto, Optica **7**, 813 (2020).

[51] J. T. Young, T. Boulier, E. Magnan, E. A. Goldschmidt, R. M. Wilson, S. L. Rolston, J. V. Porto, and A. V. Gorshkov, Phys. Rev. A **97**, 023424 (2018).

[52] Where the relevant $|S_\nu^q|$ are $\sim$1, and do not change the position of the discussed resonances.

[53] M. Kalinowski, Y. Wang, P. Bienias, M. J. Gullans, D. P. Ornelas-Huerta, A. N. Craddock, S. L. Rolston, J. V. Porto, H. P. Büchler, and A. V. Gorshkov, arXiv:2010.09772.

[54] N. Jia, N. Schine, A. Georgakopoulos, A. Ryou, L. W. Clark, A. Sommer, and J. Simon, Nat. Phys. **14**, 550 (2018).

[55] F. M. Gambetta, W. Li, F. Schmidt-Kaler, and I. Lesanovsky, Phys. Rev. Lett. **124**, 043402 (2020).

[56] M. J. Gullans, Ph.D. thesis, Harvard University, Cambridge, Massachusetts, 2013.